

Article

Simulation Analysis of Mechanical Fluidized Bed in Adsorption Chillers

Wojciech Kalawa *, Karol Sztékler , Agata Mlonka-Mędrala , Ewelina Radomska , Wojciech Nowak ,
Łukasz Mika , Tomasz Bujok  and Piotr Boruta 

Faculty of Energy and Fuels, AGH University of Science and Technology, Mickiewicza 30, 30-059 Krakow, Poland; sztekler@agh.edu.pl (K.S.); amlonka@agh.edu.pl (A.M.-M.); radomska@agh.edu.pl (E.R.); wnowak@agh.edu.pl (W.N.); lmika@agh.edu.pl (Ł.M.); bujok@agh.edu.pl (T.B.); boruta@agh.edu.pl (P.B.)

* Correspondence: kalawa@agh.edu.pl

Abstract: Adsorption systems are alternatives to compressor cooling systems. Apart from many advantages, these systems are characterized by low COP and SCP parameters. One of the most promising options to improve the performance of adsorption chillers is the replacement of the stationary bed with a fluidized one. A fluidized bed significantly increases the heat and mass transfer within the bed, enables better contact between gas and solid phases, and results in the proper mixing of adsorbent particles. This paper presents the possibility of using fluidized beds in adsorption chillers. This paper shows the results of CFD numerical modelling of the operation of a fluidized bed for an adsorption chiller and simulations of the bed temperature profiles during the adsorption and desorption processes of sorbent in a fluidized bed. This article presents an analysis of CFD simulation results for the optimal angle of heat exchangers.

Keywords: adsorption chiller; fluidization; adsorption; desalination; CFD



Citation: Kalawa, W.; Sztékler, K.; Mlonka-Mędrala, A.; Radomska, E.; Nowak, W.; Mika, Ł.; Bujok, T.; Boruta, P. Simulation Analysis of Mechanical Fluidized Bed in Adsorption Chillers. *Energies* **2023**, *16*, 5817. <https://doi.org/10.3390/en16155817>

Academic Editor: Eliseu Monteiro

Received: 26 June 2023

Revised: 25 July 2023

Accepted: 3 August 2023

Published: 5 August 2023



Copyright: © 2023 by the authors. Licensee MDPI, Basel, Switzerland. This article is an open access article distributed under the terms and conditions of the Creative Commons Attribution (CC BY) license (<https://creativecommons.org/licenses/by/4.0/>).

1. Introduction

The changing climate, together with the progress of civilisation, is driving an increase in demand for cooling. The most commonly used electrically driven compressor cooling systems are characterised by a high energy demand. Meeting the growing demand for cooling would therefore involve an increase in electricity consumption for cooling purposes. Considering that electricity is mainly produced from non-renewable sources [1], it would be true to say that, in that case, the refrigeration sector indirectly contributes to accelerating adverse climate changes. An alternative solution to the use of conventional chillers is adsorption chillers powered by low-temperature heat below 90 °C [2]. They are characterised by very low energy requirements. The heat to run an adsorption chiller can be recovered from various industrial processes emitting waste heat or obtained via solar energy conversion [3,4]. Adsorption chillers are distinguished by many advantages, including easy and quiet operation and few moving mechanical parts [5]. Despite numerous advantages, there are also serious limitations that make them less attractive and competitive compared to electrically driven compressor chillers. They are characterised by low performance coefficients, including a low cooling coefficient of performance (COP), which typically does not exceed 0.6, and a low specific cooling power (SCP) [3,6]. Consequently, this contributes to the large weight and dimensions of the equipment [4,7]. Therefore, it is necessary to search for opportunities to improve the efficiency of adsorption chillers. The increase in demand for cooling has led to an increased interest in adsorption chillers. As a result, an increasing number of scientific articles have focused on exploring new opportunities to improve the performance of adsorption chillers.

The most important parameters characterizing the performance of adsorption chillers are the cooling COP (coefficient of performance) and SCP (specific cooling power). For chillers with desalination function, the SDWP (specific daily water production) is also very

important as it specifies the amount of desalinated water per unit of adsorbent mass per day [8]. It is affected by many factors, such as the bed regeneration temperature, chilled water temperature, and cycle time. The efficiency of a cooler also depends on its design and the working pair used. In particular, it is related to the properties of the sorbent. Improved efficiency of adsorption chillers can be achieved in many ways, including the following:

- choice of modern sorption materials [6];
- improved heat transfer in the sorbent [9];
- improved heat transfer at the interface between the sorbent and the heat exchanger [6,10,11];
- use of internal heat recovery [4,12];
- selection of the optimum duration of the half-cycle [13];
- use of an appropriate number of beds [12];
- fluidisation of the adsorbent bed [14].

One of the biggest problems with the most commonly used highly porous sorption materials is their very low coefficient of thermal conductivity. This results in poor heat transfer within the bed and, consequently, a lower performance of the entire unit [5]. One way to increase the performance of an adsorption chiller is to improve the heat transfer within the bed [9]. This can be achieved in many ways. The first is the choice of modern adsorbents [6]. Material science is constantly developing, thus providing more and more possibilities. The ideal sorbent material combines good thermal conductivity and high sorption capacity. Currently, the choice of a suitable adsorbent is dictated by the cost-effectiveness of the device and involves a search for a compromise between a high coefficient of thermal conductivity and a high sorption capacity [5]. However, there are available materials that are characterised by a large specific surface area and pore volume without losing good thermal conductivity properties. Such materials include, e.g., hybrid MOFs (metal–organic frameworks) [6].

Enhanced heat transfer inside the bed can also be achieved by doping the sorbents with materials with a higher heat transfer coefficient [9]. The effect of using polydispersity will be a replacement of gas voids between sorbent grains. Inter-grain spaces have a particularly negative effect on heat transfer inside the bed as the heat transfer coefficient of still air is even lower than that of silica gel, at 0.025 W/(mK) [6]. Research results indicate a clear intensification of the processes of adsorption and desorption of the silica gel mixture with an appropriate percentage of a metal additive compared with the reference sample and, at the same time, a slight loss of sorption properties [9].

Heat transfer is significantly reduced at the adsorbent–heat exchanger interface. This is caused by a significant difference between the heat transfer coefficients of the adsorbent and those of the heat exchanger material. An effective method to increase heat transfer in the boundary zone is to coat the silica gel layer in contact with the heat exchanger surface with a binder [6]. The most important component responsible for heat exchange is the one in which the heating/cooling water flows in the heat exchanger. Its design can greatly affect the performance of the entire unit [10].

The performance of an adsorption chiller will also be higher for devices that allow internal heat recovery after bed regeneration and use the cooling water previously used to cool one bed to preliminarily reduce the temperature of the other bed [4,12]. Many advanced heat recovery cycles have been proposed in the course of many studies, and these include the thermal wave cycle, the forced convection thermal wave cycle and the cascade cycle [4].

A very important and relatively easily modifiable parameter of chiller operation with a great influence on its efficiency and power is the duration of half-cycles [13]. The length of this time determines how much adsorbate will flow from the evaporator to the bed and from the bed to the condenser. The switching between half-cycles should take place at a time corresponding to the actual completion of adsorption or desorption. If the time of adsorption is too short, too little adsorbate will be adsorbed on the sorbent surface and too little refrigerant will evaporate to the condenser, thus contributing to lower distillate production or too low chilled water temperature. On the other hand, if the desorption time

is too long, the energy supplied to the bed in the regeneration process will be irretrievably lost [15].

The use of multi-bed systems ensures continuous operation and results in the greater stability of the chiller operation, increased cooling power and higher COP and SDWP [6,12,16,17]. An experiment was carried out during which a system with four and six beds was tested under the same conditions. The results show that the use of four beds enabled a 70% increase in the cooling capacity coefficient in comparison with a device with two beds, while the operation of six beds was characterised by a COP value 40% higher than for a chiller using only four beds [12].

The most commonly used adsorption chillers are equipped with stationary (fixed) beds, which means that there is silica gel packed inside between the tubes of the heat exchanger. This, to a large extent, limits heat and mass transfer within the bed [14,18]. In adsorption chillers, the bed is the structural component where the sorbent fills the heat exchanger, which is usually a closed structure by using a stainless steel mesh with a mesh diameter smaller than the sorbent used. The heat exchanger, which is filled with sorbent, is where the heat transfer between the cooling/heating medium takes place during the process of adsorption or desorption (finned tube or tube heat exchanger). The heat transfer is significantly reduced at the adsorbent–heat exchanger interface. This is caused by the significant difference between the heat conductivity coefficients of the adsorbent and the heat exchanger material. The problem of high thermal resistance is due to the poor heat conduction of the adsorbents used, and the presence of numerous voids between the sorbent particles [6,9]. Further barriers are the heat exchanger material itself and the physics of the processes. This contributes to a significant increase in adsorption and desorption times. This results, among other things, in the low specific cooling power (SCP) and the large size and weight of the equipment [18]. The use of efficiency-enhancing methods, e.g., an appropriate heat exchanger design, can partially reduce the weak points of adsorption chillers. This type of issue is described in more detail in the section above. For fixed-bed adsorption chillers, the COP values of the equipment are shown in Table 1.

Table 1. Summary of parameters of selected adsorption chillers [6–9].

No.	Working Pair	Hot Water Temperature °C	Cold Water Temperature °C	SCP W/kg	SDWP m ³ /Tonne	COP	Details
1	Silica gel–water	85.0	24.0	30.2	0.96	0.28	two-stage, four-bed
2		70.0	16.0	12.3	-	0.23	
3		70.0	27.6	-	9.97	-	four-bed, int. heat recovery
4		85.0	30.0	112.0	4.0	0.46	two-bed, solar heat-driven
5		85.0	25.0	~140.0	5.3	~0.50	
6		85.0	15.0	~225	8.0	~0.55	
7		60.0	25.0	-	-	0.64	three-bed
8		85.5	29.5	125.0	-	0.51	two-bed with optimized modular
9		85.4	30.3	86.4	-	0.34	

In the literature, there are many examples of many different heat exchangers used in adsorption chillers. The most common designs include the following:

- Finned-tube heat exchangers, which consist of a single tube or a multi-tube system of straight or U-shaped tubes that are finned on the outside. The adsorbent is placed between the fins, and the whole is inserted into a special mesh that holds all the components together.
- Plate finned-tube heat exchanger. This heat exchanger consists of longitudinal manifolds connected by smaller diameter tubes forming a meandering ‘finning’ in order

to increase the heat transfer surface. The tubes are connected to each other by means of fin plates. The entire heat exchange assembly is placed in a frame with a mesh which prevents the adsorbent from moving freely in the structure. With this exchanger, the device achieved a COP value of 0.48, with SCP from 208 W/kg_{ads} to 590 W/kg_{ads} [19,20].

- Finned flat-tube heat exchanger is a structure consisting of flattened tubes connected by a dense mesh arranged in alternately overlapping triangular-shaped fins. The spaces between the fins are filled with adsorbent and enclosed in a frame. By using an appropriate granulation, it is possible to achieve a COP of 0.4 with SCP from 675 W/kg_{ads} to 2.3 kW/kg_{ads} [20].

One of the most promising options to improve the performance of adsorption chillers involves replacing a stationary bed with a fluidised one. This solution is an alternative to fixed beds. Fluidisation has been successfully used for a long time in many industries, including gas drying processes, bulk materials, product freezing and heating, solid fuel combustion, in cracking process and many others. Fluidisation of a bed can be described as a condition in which particles of the sorption material are affected by a fluid flowing through the bed at a specific fluidisation velocity u [21]. Under the influence of the air flowing from the bottom of the adsorber, a suspension of particles is formed. These particles then exhibit physical properties comparable to liquids [22]. The fluidisation velocity cannot be too low as this will mean the desired fluidisation phenomenon will not occur and the particles will remain stationary. The minimum critical fluidisation velocity u_{cr} is required for the particles to begin to rise and form a fluidised layer [22]. On the other hand, the fluidisation velocity cannot be too high (lower than the particle entrainment velocity) because this could lead to blockage of the flow from the bed to the evaporator [23]. It is therefore a very important parameter in the design of fluidised beds [24].

Numerous studies also indicate that a fluidised bed adsorption chiller is characterised by better heat and mass transfer. Adsorption and desorption processes are then much more intense [25]. A shorter cycle time is associated with an increase in cooling power and an increase in COP and SCP. The maximum adsorption rate is observed at the beginning of the process and decreases with time [26].

Tests have also been carried out to determine the value of the coefficient of heat transfer between the surface of the heat exchanger and the bed for fixed and fluidised beds. The results are presented in [27]. The heat transfer coefficients for fixed and fluidised beds for a gas velocity of 0.03 m/s were 7.29 W/(m²K) and 280.89 W/(m²K), respectively [27]. Furthermore, this coefficient was shown to increase with decreasing grain size [27].

It was also shown that as the velocity of the medium reaching the bed increased, an increase in the amount of adsorbed adsorbate and the rates of adsorption and desorption was noticeable [25]. The adsorption and desorption efficiency also increases with the increasing height of bed packing [27]. The amount of adsorbed water increases with increasing adsorbent mass in the bed [26]. The particle size affects the value of the minimum fluidisation velocity and the COP of the chiller. According to the equation for the minimum velocity required to form a fluidised bed and the tests conducted, it increases with increasing particle size [23,24]. It was also observed that a more spherical particle shape causes the minimum fluidisation velocity to increase [24]. The velocity is also affected by the height and diameter of the bed [24]. Furthermore, it decreases when the pressure increases. As the diameter of the adsorbent particles decreases, the thermal COP of the device increases [23]. The motion of the particles inside the bed is influenced among other things by the design of the manifold and the degree of slope of the inlet to the adsorber causing particle turbulence [28].

However, fluidisation can be achieved even under high vacuum conditions [29]. It is bubbling in nature. The hydrodynamic conditions are similar to those of fluidisation under high pressure [29].

It was also noted that, for a fluidised bed, more water is adsorbed on the surface of the silica gel than for a fixed bed packed with it [27]. This is due to the fact that in a fluidised

bed, a larger sorbent surface area can be in contact with the adsorbate. A fixed bed has a smaller total active surface area of the sorbent due to the high packing of the material [27]. Fluidisation also makes it possible to carry out a more efficient regeneration of the bed at a lower temperature, which is associated with high mass and heat transport efficiency [27].

Simulations in ANSYS software of the operation of an adsorption chiller using a mechanical fluidized under vacuum conditions have not been previously analysed by other researchers; thus, this research is innovative. Simulation calculations as well as experimental studies make it possible to analyse the processes occurring during sorption and desorption during fluidization in the adsorption chiller bed. The fluidization process is carried out in a bed characterized by a unique design which has not previously been used in adsorption chillers, and the simulation results obtained will enable further development of this type of design, thus improving the efficiency of cooling equipment.

2. Materials and Methods

2.1. Mathematical Model

Fluidised bed adsorption chillers were modelled in the ANSYS software, and the sorption/desorption process as well as heat transfer between the sorbent particles and the surface of the heat exchanger were analysed.

Obtaining reliable results of the analysis is largely dependent on the appropriate selection and implementation of models allowing for a numerical simulation of the phenomena occurring in a real system. These equations, in combination with the number of elements, affect the accuracy of the results and the length of the calculations. It is necessary to present the accuracy of the model and to take into account the limited computing power and finite simulation time.

For all flow phenomena, Ansys Fluent solves the equations of conservation of mass and momentum. In the presence of heat transfer or flow compressibility, it is also necessary to consider energy conservation. In the flows involving mixing and reactions of substances, the equation of substance conservation is added to the system of equations. Additionally, if the flow is turbulent, the turbulence equations are solved [30–34].

The conservation of mass equation, also called the continuity equation, is written as follows (1):

$$\frac{\partial \rho}{\partial t} + \nabla \cdot (\rho \mathbf{v}) = S_m \quad (1)$$

This is the general form of the equation valid for compressible and incompressible flows. The S_m source represents the portion of the mass added to the continuous phase, e.g., vaporization of liquid droplets in the gas phase. The source can be described as in Equation (2) for axisymmetric problems, as follows:

$$\frac{\partial \rho}{\partial t} + \frac{\partial}{\partial x}(\rho v_x) + \frac{\partial}{\partial r}(\rho v_r) + \frac{\rho v_r}{r} = S_m \quad (2)$$

where x is the axial coordinate, r —radial, v —velocities in the respective coordinates. The equation of conservation of momentum is as in Formula (3), as follows:

$$\frac{\partial}{\partial t}(\rho \bar{\mathbf{v}}) + \nabla \cdot (\rho \bar{\mathbf{v}} \mathbf{v}) = -\nabla p + \nabla \cdot (\bar{\boldsymbol{\tau}}) + \rho \bar{\mathbf{g}} + \bar{\mathbf{F}} \quad (3)$$

where p is the static pressure, $\bar{\boldsymbol{\tau}}$ the stress tensor, $\rho \bar{\mathbf{g}}$ represents the force of gravity, and $\bar{\mathbf{F}}$ the external mass forces acting on the fluid, depending on the model adopted. The stress tensor is described as in the formula (4), as follows:

$$\boldsymbol{\tau} = \mu[\nabla \mathbf{v} + \nabla \mathbf{v}^T - 2/3 \nabla \cdot \mathbf{v} \mathbf{I}] \quad (4)$$

In Ansys Fluent, it is possible to include heat transfer in a flow. The energy equation takes the following form (5):

$$\frac{\partial}{\partial t}(\rho E) + \nabla(\bar{v}(\rho E + p)) = \nabla \cdot (k_{\text{eff}} \nabla T - \sum_j h_j \bar{J}_j + \bar{\tau}_{\text{eff}} \cdot \bar{v}) + S_h \quad (5)$$

where k_{eff} expresses the effective conduction coefficient ($k + k_t$, where k_t is the turbulent conduction coefficient defined depending on the turbulence model used), and \bar{J}_j expresses the diffusive flux of the substance. Successive parts of Equation (5) define the energy transfer through conduction, the substance diffusion, and the viscous dissipation. The term S_h is user-defined volumetric heat sources.

The quantity E from Equation (5) is defined as follows (6):

$$E = h - \frac{p}{\rho} + \frac{v^2}{2} \quad (6)$$

where h expresses enthalpy. For ideal gases, it is defined as follows (7):

$$h = \sum_j Y_j h_j \quad (7)$$

However, for incompressible flows, it is as follows:

$$h = \sum_j Y_j h_j + \frac{p}{\rho} \quad (8)$$

The quantity Y_j appearing in Equations (7) and (8) expresses the mass fraction of a given substance. The enthalpy of the j -th substance is calculated from the following formula (9):

$$h_j = \int_{T_{\text{ref}}}^T c_{p,j} dT \quad (9)$$

The reference temperature T_{ref} depends on the solver and the models used.

As heat is applied to a fluid, its density changes in proportion to the temperature change. This leads to the creation of a flow under the influence of gravity acting on the fluid, the density of which changes (buoyancy-driven flow). This type of flow is known as natural (or mixed) convection. The influence of buoyancy forces on the share of free and forced convection in the flow determines the mutual ratio of the Grashof and Reynolds numbers (10)

$$\frac{Gr}{Re^2} = \frac{g\beta\Delta TL}{v^2} \quad (10)$$

When the value of the above Equation (10) is close to or greater than one, the proportion of displacement in the flow is significant. For very small values, the buoyancy forces may be neglected in the model.

For the strictly natural convection mechanism, the mean of the flow can be determined by the Rayleigh number (11), as follows:

$$Ra = \frac{g\beta\Delta TL^3 \rho}{\mu\alpha} \quad (11)$$

where β is the thermal expansion coefficient (12), while α is the thermal diffusivity coefficient (13).

$$\beta = -\frac{1}{\rho} \left(\frac{\partial \rho}{\partial T} \right)_p \quad (12)$$

$$\alpha = \frac{k}{\rho c_p} \quad (13)$$

Turbulence—realizable k - ϵ assuming a medium-steady turbulent fluid motion, each of the flow parameters at a given time can be written as the sum of the averaged value and its fluctuations. For a given speed component, this notation takes the following form:

$$u_i = \bar{u}_i + u_i' \quad (14)$$

We record scalar quantities in the same way, as follows:

$$\phi_i = \bar{\phi}_i + \phi_i' \quad (15)$$

where ϕ denotes scalar quantities such as pressure, energy, or concentration.

Adopting a description of a mean steady motion leads to the following form of the transport equations (i.e., the continuity and moment equation) in the tensor notation:

$$\frac{\partial \rho}{\partial t} + \frac{\partial}{\partial x_i} (\rho u_i) = 0 \quad (16)$$

$$\frac{\partial}{\partial x_i} (\rho u_i) + \frac{\partial}{\partial x_j} (\rho u_i u_j) = -\frac{\partial p}{\partial x_i} + \frac{\partial}{\partial j} \left[\mu \left(\frac{\partial u_j}{\partial x_j} + \frac{\partial u_j}{\partial x_i} - \frac{2}{3} \delta_{ij} \frac{\partial u_j}{\partial x_j} \right) \right] + \frac{\partial R_{ij}}{\partial x_j} \quad (17)$$

where R_{ij} is the Reynolds stress tensor related to the averaged velocity of the momentum change due to turbulent pulsations. In the Cartesian coordinate system, this tensor takes the following form, as shown in Equation (18):

$$R_{ij} = -\overline{\rho u_j' u_i'} = \begin{bmatrix} -\overline{\rho (u_x')^2} & -\overline{\rho u_x' u_y'} & -\overline{\rho u_x' u_z'} \\ -\overline{\rho u_y' u_x'} & -\overline{\rho (u_y')^2} & -\overline{\rho u_y' u_z'} \\ -\overline{\rho u_z' u_x'} & -\overline{\rho u_z' u_y'} & -\overline{\rho (u_z')^2} \end{bmatrix} \quad (18)$$

The system of Equations (16) and (17) is not a closed system. In the Reynolds tensor, there are no six equations defining the individual components. In this commissioned work, the problem of setting up additional equations was solved by calculating the effect of turbulence according to the Boussinesq approach [34]. According to this hypothesis, there is a relationship between the components of the Reynolds tensor and the deformation velocity tensor. In the index notation, this relationship is expressed by Equation (19).

$$R_{ij} = -\overline{\rho u_j' u_i'} = \mu_T \left(\frac{\partial \bar{u}_i}{\partial x_j} + \frac{\partial \bar{u}_j}{\partial x_i} \right) - \frac{2}{3} \left(\rho k + \mu_T \frac{\partial u_k}{\partial x_k} \right) \delta_{ij} \quad (19)$$

The turbulence model adopted in the calculations is the “Realizable k - ϵ model”, loosely translated as the solvable k - ϵ model. It is characterized by the fact that it has implemented modified equations describing the turbulent viscosity and the speed of energy dissipation compared to the traditional model. The term “solvable” reflects a feature of the model by satisfying certain mathematical conditions in terms of Reynolds stresses consistent with the physics of turbulent flow.

Equations describing the kinetic energy of turbulence (20) and its dissipation (21) are as follows:

$$\frac{\partial}{\partial t} (\rho k) + \frac{\partial}{\partial x_i} (\rho k u_i) = \frac{\partial}{\partial x_i} \left[\left(\mu + \frac{\mu_t}{\sigma_k} \right) \frac{\partial k}{\partial x_j} \right] + G_k + G_b - \rho \epsilon - Y_M + S_k \quad (20)$$

$$\frac{\partial}{\partial t} (\rho \epsilon) + \frac{\partial}{\partial x_j} (\rho \epsilon u_j) = \frac{\partial}{\partial x_j} \left[\left(\mu + \frac{\mu_t}{\sigma_\epsilon} \right) \frac{\partial \epsilon}{\partial x_j} \right] + \rho C_{1\epsilon} S \epsilon - \rho C_{2\epsilon} \frac{\epsilon^2}{k + \sqrt{\nu \epsilon}} + C_{1\epsilon} \frac{\epsilon}{k} C_{3\epsilon} G_b + S_\epsilon \quad (21)$$

where:

$$C_1 = \max \left[0.43; \frac{\eta}{\eta + 5} \right]; \eta = S \frac{k}{\epsilon} \quad (22)$$

In the above equations, G_k represents the generation of kinetic energy of turbulence through the averaged values of the velocity gradients (23), as follows:

$$G_k = -\rho \overline{u_i' u_j'} \frac{\partial u_j}{\partial x_i} \quad (23)$$

G_b is the generation of kinetic energy of turbulence due to buoyancy forces, according to the following formula (24):

$$G_b = \beta g_i \frac{\mu_t}{Pr_t} \frac{\partial T}{\partial x_i} \quad (24)$$

where Pr_t is the turbulent Prandtl number for the adopted model amounting to 0.85, and g_i is the acceleration vector due to gravity. The thermal expansion coefficient is defined by the formula (12).

Another variable, denoted as Y_M , which takes into account the compressibility in the flow, is particularly significant in flows for which the Mach number is greater than one. The formula that defines this variable can be presented as follows (25):

$$Y_M = 2\rho\epsilon Ma_t^2 \quad (25)$$

The variable Y_M is a turbulent Mach number, defined as follows (26):

$$Ma_t = \sqrt{\frac{k}{a^2}} \quad (26)$$

The variable $C_{3\epsilon}$ shows to what extent the energy dissipation depends on the buoyancy forces. It takes the following form (27):

$$C_{3\epsilon} = \tanh \left| \frac{v}{u} \right| \quad (27)$$

where v is the velocity component parallel to the acceleration vector due to gravity, and u perpendicular to the acceleration due to gravity. $C_{3\epsilon}$ takes the value equal to one in a flow, where the main direction of the flow and the gravity vector are consistent, and in the case of the perpendicular arrangement of these vectors, the zero value.

The other variables in the formula for the energy dissipation speed ϵ are constants, namely, turbulent Prandtl numbers, $\sigma_k = 1$ and $\sigma_\epsilon = 1.2$, defined separately for the equation for turbulence kinetic energy and energy dissipation, constants $C_{1\epsilon} = 1.44$ and $C_2 = 1.9$ and user-defined source functions S_k, S_ϵ .

A key issue in modelling is the proper definition of turbulent viscosity. The solvable model $k-\epsilon$ turbulent viscosity is calculated according to the following formula (28):

$$\mu_t = \rho C_\mu \frac{k^2}{\epsilon} \quad (28)$$

Contrary to the standard $k-\epsilon$ model, in the solvable $k-\epsilon$ model, the quantity C_μ ceases to be a constant (29), as follows:

$$C_\mu = \frac{1}{A_0 + A_s \frac{kU^*}{\epsilon}} \quad (29)$$

where:

$$U^* = \sqrt{S_{ij}S_{ij} + \tilde{\Omega}_{ij}\tilde{\Omega}_{ij}} \quad (30)$$

$$\tilde{\Omega}_{ij} = \Omega_{ij} - 2\epsilon_{ijk}\omega_k \quad (31)$$

$$\Omega_{ij} = \overline{\Omega}_{ij} - \epsilon_{ijk}\omega_k \quad (32)$$

$$S_{ij} = \frac{1}{2} \left(\frac{\partial u_j}{\partial x_i} + \frac{\partial u_i}{\partial x_j} \right) \quad (33)$$

$\overline{\Omega}_{ij}$ represents the average tensor rotation speed from the point of view of the rotating coordinate system with the angular velocity ω_k . Constant $A_0 = 4.04$. The constant A_s is represented by the following formula (34):

$$A_s = 6 \cos \phi \quad (34)$$

where:

$$\phi = \frac{1}{3} \cos^{-1}(\sqrt{6}W) \quad (35)$$

$$W = \frac{S_{ij}S_{jk}S_{ki}}{\tilde{S}} \quad (36)$$

$$\tilde{S} = \sqrt{S_{ij}S_{ij}} \quad (37)$$

As can be seen, the constant C_μ takes into account the mean angular velocity of the fluid, the mean deformation velocity, and the angular velocity.

In order to model the multiphase flow, the "Species Transport" model was selected for the calculations. It describes the convective diffusion of the mass to the volume chosen as the base. The diffusion equation takes the following form (38):

$$\frac{\partial}{\partial t}(\rho Y_i) + \nabla \cdot (\rho \bar{v} Y_i) = -\nabla \cdot \bar{J}_i + R_i + S_i \quad (38)$$

where Y_i is the mass fraction of the i substance in the mixture, R_i the rate of increase/reduction in the substance as a result of a chemical reaction, S_i rate of increase/reduction in the substance as a result of adding it to the process. In turbulent flows, the diffusion flux of a substance is determined according to the following formula (39):

$$\bar{J}_i = - \left(\rho D_{i,m} + \frac{\mu_t}{Sc_t} \right) \nabla Y_i \quad (39)$$

where $D_{i,m}$ is the diffusion coefficient for the i -th substance in the mixture, the turbulent viscosity coefficient is described by Equation (28), and Sc_t is the turbulent Schmidt number, by default assumed at 0.7.

During the construction of geometric models, the following simplifications were made:

- The housing of the elements has been simplified to the form of a cylinder, without sight glasses and measuring connectors.
- Irregularly shaped elements such as heating and cooling junction boxes in the evaporator and condenser are simplified to a cylinder form.
- For the sorption chamber, the structural elements supporting the bed were omitted, and the bed itself was simplified to the form of a cuboid.

Then, after creating the structural elements, they were filled with the fluid domain in order to obtain the appropriate computational domains constituting the interior of the sorption chamber, evaporator, and condenser, respectively.

After developing the geometric model of the bed, it was exported to the ANSYS Meshing module. Using the ANSYS Meshing module, the continuous domain was discretized to

obtain a computational grid. To assess the quality of the grid, an analysis of cells' quality parameters was carried out, and the following was found:

- Orthogonal quality: value is in the range $<0, 1>$, value 1 stands for the highest possible quality.
- Skewness: value is in the range $<0, 1>$, value 0 stands for the highest possible quality.

The orthogonal quality for most elements (about 70% of the elements) was estimated to be in the range of 0.73–1.0. Similarly, the skewness for most elements (about 70% of the elements) was estimated to be in the range of 0–0.25. The meshes have 350,464 nodes and 1,673,113 elements. It has an average orthogonality of 0.787 with a deviation of 0.14 and an average skewness of 0.23 with a deviation of 0.13. About 1% of the elements have an orthogonality value of less than 0.5, and about 85% of the elements have an orthogonality greater than 0.75. The Realisable k - ϵ turbulence simulation model with a standard wall function was chosen because it is well-known and successfully used in adsorption simulation. In addition, due to the multiphase flow that is characteristic of the phenomenon being simulated, the Dense Discrete Phase Model (DDPM), which works in Euler–Lagrange terms, was chosen. With this model, the momentum equations are not calculated for each individual particle, but for a certain set of particles related to each other by specific physical dimensions. The DDPM model can be used together with the k - ϵ turbulence simulation model.

2.2. Physical Model

A specially designed model of an experimental installation was prepared for the solution applied. The parameters of cooling and heating water, and the pressure range that were selected during the process of modelling sorption/desorption for the fluidised bed chiller correspond to the operating conditions of the stationary bed device. These data are presented in the section on the performance of an experimental solid bed adsorption chiller [3,35,36]. A silica gel sorbent was used for simulation and experimental studies, the parameters of which are shown in Table 2.

Table 2. Physical parameters of the sorbent used.

Parameter	Value
Granulation, μm	400–800
Specific surface area, m^2/g	750–830
Bulk density, kg/m^3	755
Actual density, kg/m^3	2200
Regeneration temperature, $^{\circ}\text{C}$	<90
Average pore diameter, nm	2–3
Specific thermal capacity, J/kgK	924
Thermal conductivity, W/mK	0.175

Within the framework of the model-based testing, the thermal and flow phenomena taking place inside the sorption chamber were determined with a particular emphasis on the kinematics of silica gel in the processes of sorption and desorption. The amount of sorbent subjected to fluidisation is 1.3 kg at a velocity (normal to the inlet surface) of 0.04 m/s and mass flow rate of 0.1 kg/s. A diagram of the test installation with a mechanical bed is present in Figure 1.

The movement of the adsorbents, which was forced mechanically, causes a number of problems during the cyclic operation of the beds in the chiller, and, as such, a solution is not commercially available on the market so far. The heat exchanger, together with the mechanical bed, works under vacuum, and the pressure is maintained by a system of vacuum pumps, ensuring the right working conditions. Therefore, for the purpose of

evaluating the results of the simulation calculations presented in this paper, single real-world tests were performed within the adsorption cycle and within the desorption cycle on the experimental chiller, which were repeated several times. The upward movement of the adsorbent is forced by a screw feeder. From the top, due to the sloped construction of the bed, the adsorbent flows towards the screw feeder tank. During this time, heat and mass exchange processes take place.

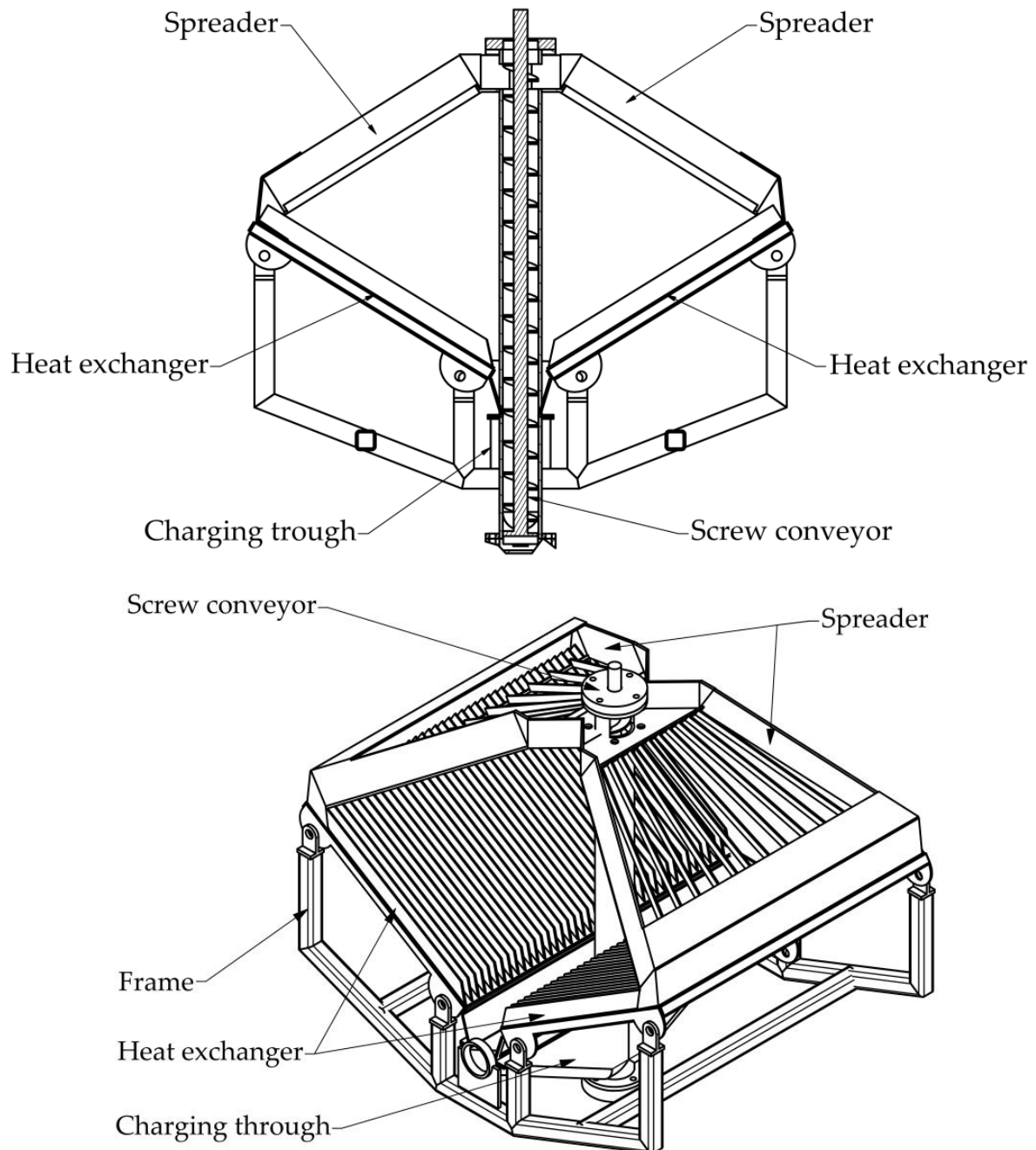


Figure 1. Cont.

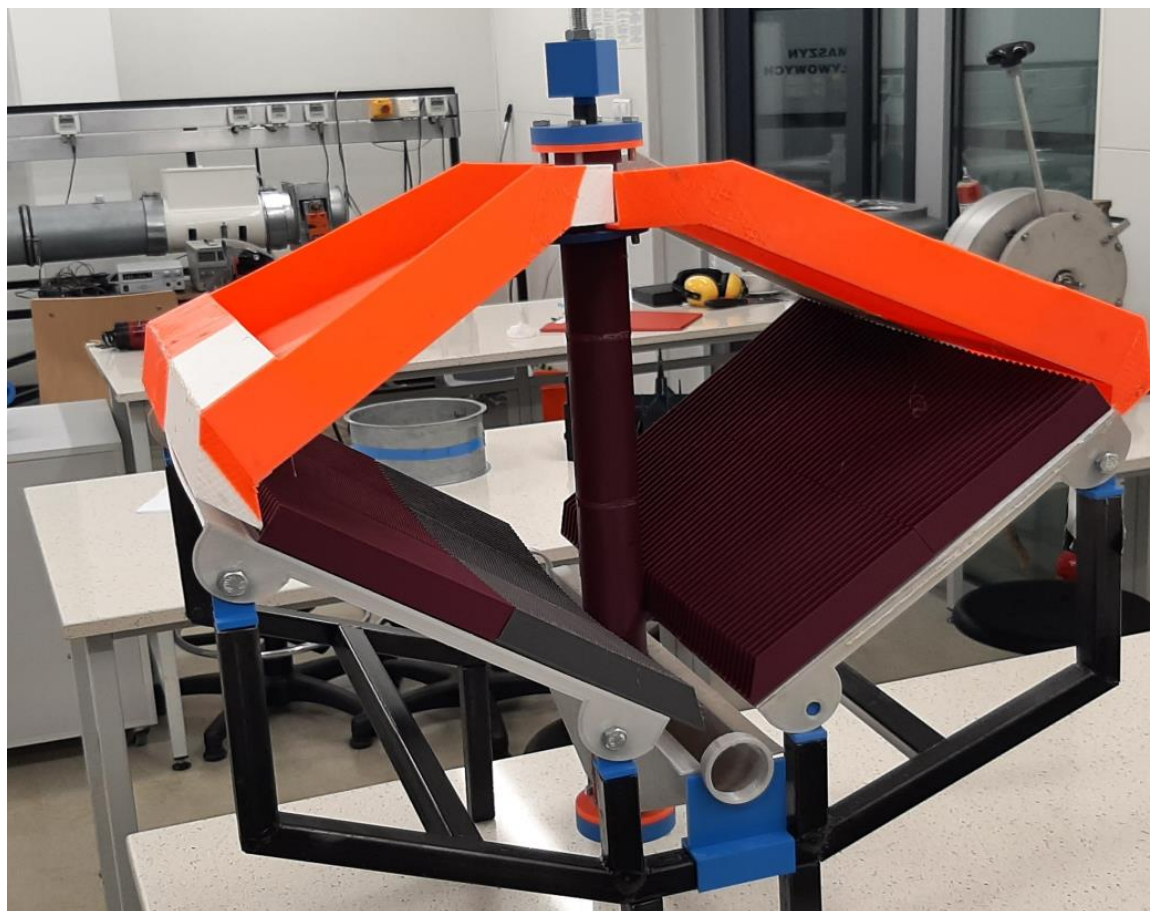


Figure 1. Diagram and figure of the test installation mechanical CFB.

3. Results—Model of CFD Fluidized Mechanical Bed

Simulation calculations of a mechanical fluidised bed for adsorption and desorption processes are presented below. The boundary conditions for the simulation of a mechanical fluidised bed were determined via experimental studies based on the operation of a real system. The assumptions for the model's accuracy were outlined in an earlier chapter. Simulation calculations focused on the temperature distribution between sorbent particles contacting the exchanger during the adsorption and desorption phases. The calculations were carried out for one variant of the exchanger inclination angle in bed of adsorption chiller.

3.1. Adsorption

The adsorption process is exoenergetic in nature; therefore, for this process to take place efficiently, the heat released from the sorbent must be removed, which is related to the characteristics of the sorbent. The removal of heat from the silica gel takes place through a heat exchanger through which the cooling water flows. In the case under consideration, the cooling processes of the silica gel particles are modelled. A cooling medium flows through this exchanger, removing heat from the silica gel particles. In the model-based testing, a constant heat transfer was determined at the edges of the heat exchanger. The graphs below show simulations of heat removal during the sorption process. Graphs below (Figures 2 and 3) show the mechanical the bed with silica gel particles and the distribution and temperature of the particles at different time intervals (6 s and 12 s). The graphs presented show the initial non-stationarity of the process. For 6 s, no change in silica gel temperature at the outlet of the bed was observed (mainly average temperature at the outlet); this was visible at 12 s, where exchanger inclination angle is 43° .



Figure 2. Distribution and temperature of particles at 6 s.

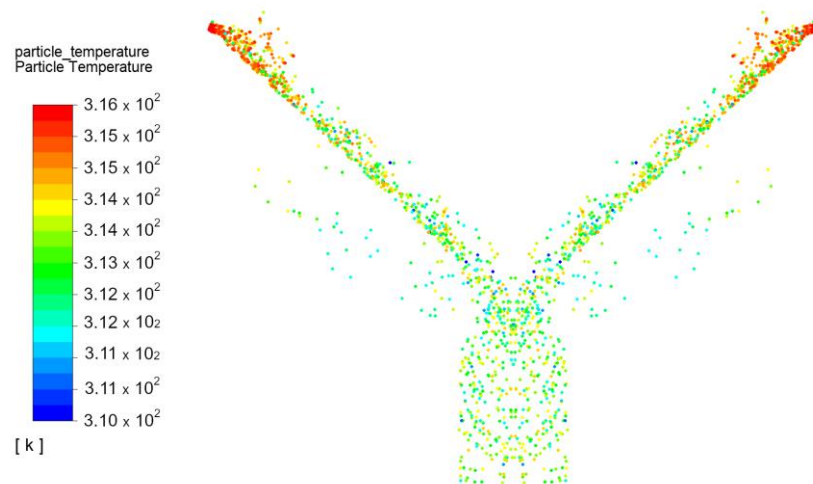


Figure 3. Distribution and temperature of particles at 12 s.

For the specified boundary conditions, the decrease in the average temperature of silica gel during the sorption process after heat removal is $3.8\text{ }^{\circ}\text{C}$. For the analysis, it was assumed that the temperature of water cooling the heat exchanger in the fluidised bed, which is washed by the fluidised sorbent, was $28\text{ }^{\circ}\text{C}$. Presented below are simulation results in the fluidised bed.

The simulation results show the following:

- Average temperature of silica gel at the inlet: $T_{\text{av in}} = 43\text{ }^{\circ}\text{C}$;
- Average temperature of silica gel at the outlet: $T_{\text{av out}} = 39.2\text{ }^{\circ}\text{C}$;
- Temperature differences between outlet and inlet: $\Delta T = -3.8\text{ }^{\circ}\text{C}$;
- Exchanger inclination angle is 43° .

Figure 4 presents the kinetic energy contour, and refers to the steady state at 12 s. By analysing the data, it can be stated that the lighter particles fluidise more intensively, which causes them to have longer contact with water vapour, contributing to a more intensive sorption process, and the direction of the particles is close to tangential in the direction of the heat exchanger.

By analysing the data, it can be stated that during the sorption process (cooling process), the highest value of the temperature drop of the sorbent is $3.8\text{ }^{\circ}\text{C}$ and is reached after 12 s.

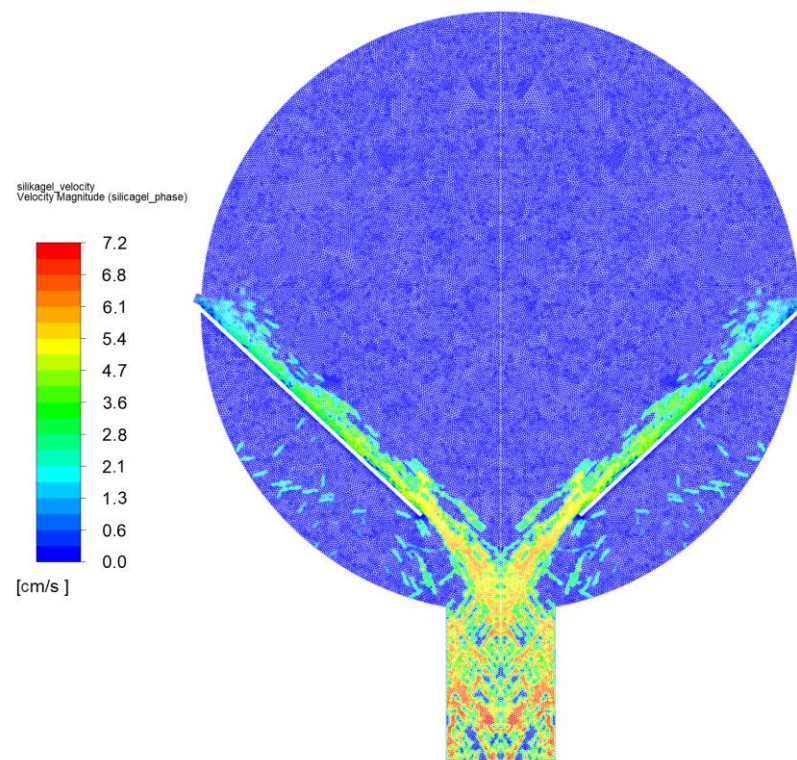


Figure 4. Velocity contour for the discrete phase at 12 s.

3.2. Desorption

The graphs presented reflect the non-stationarity of the heat transfer process and the temperature distribution in the sorbent in the mechanical fluidised bed in the desorption process. Figure 5 show the temperature distribution for 6 s, where a low intensive temperature rise in the sorbent can be observed.

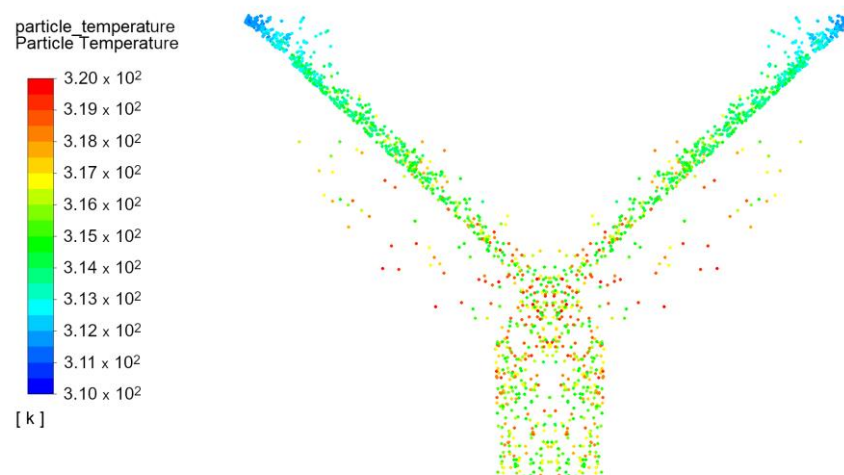


Figure 5. Distribution and temperature at 6 s.

Figure 6 presents the distribution and temperature of particles at 12 s. From the model data, it can be concluded that the temperature equilibration for the silica gel is reached after 12 s, where the sorbent particles reach their maximum temperature while washing the surface of the heat exchanger.

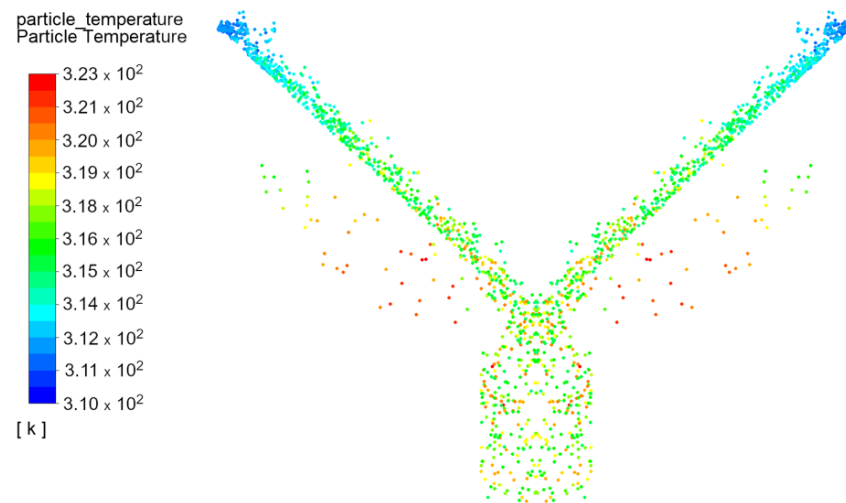


Figure 6. Distribution and temperature at 12 s.

Based on the simulation data, the temperature difference between the outlet and the inlet is approx. 4.78 °C. The assumed temperature of the exchanger is 74.89 °C. Based on the data, it is a possibility to increase the temperature of the sorbent material via multiple flows in the system.

The simulation results show the following:

- Average temperature of silica gel at the inlet: $T_{av\ in} = 39.9\text{ °C}$;
- Average temperature of silica gel at the outlet: $T_{av\ out} = 44.7\text{ °C}$;
- Increase the temperature of silica gel: $\Delta T = 4.78\text{ °C}$;
- Exchanger inclination angle is 43°.

In Figure 7, the contour of kinetic energy refers to the steady state at 12 s. By analysing the data, it can be concluded that the lighter particles reflect more intensely and fluidise, which causes them to have longer contact with the water vapour, thus contributing to a more intense desorption process.

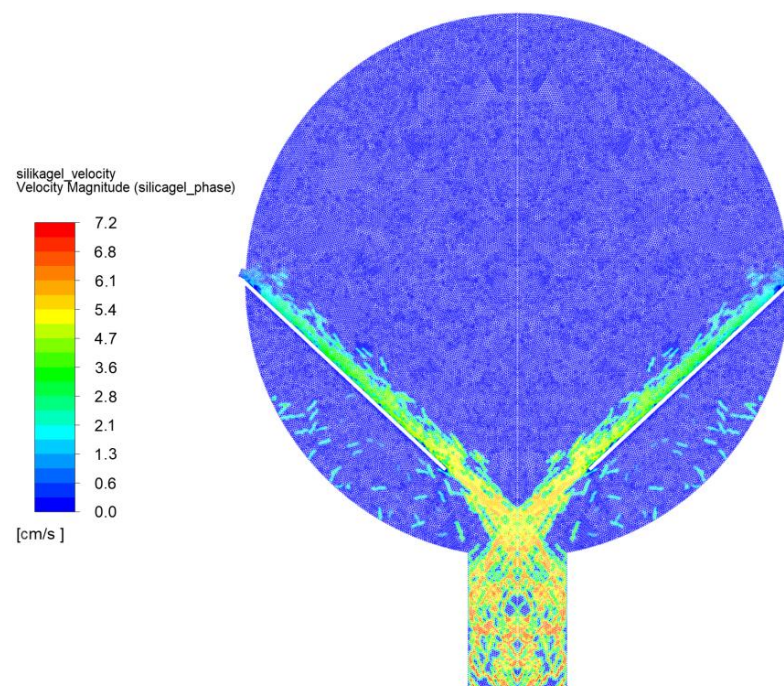


Figure 7. Velocity contour for the discrete phase at 12 s.

Based on the simulation data, high activity of sorbent particles can be observed below the exchanger surface where they come into contact with its walls. In the case of the turbulence kinetic energy contour, significant vortex structures are observed in the downstream part of the exchanger, which is related to the collision of particles on both sides of the bed.

In the heat exchanger prepared, a two-dimensional, fully parameterized model of the bed was created, and multiphase flow was incorporated, as well as heat transfer from the wall to the sorbent particles, and the occurrence of turbulence was also modelled. By analysing the data, it can be concluded that during the desorption process (heating process), the highest value of temperature rise was 4.78 °C and was reached after 6 s.

The result of the experiment between the model and the experimental study is presented in Table 3. Experimental tests were carried out on a mechanical bed, where the adsorption desorption process was studied. The conditions of the experiment corresponded to the conditions of the simulation carried out during the desorption sorption process.

Table 3. Comparison of experimental studies on a test bed with a model of a fluidal mechanical bed.

Desorption								
	Exp. 30 s	Model 30 s	Exp. 60 s	Model 60 s	Exp. 90 s	Model 90 s	Exp. 160 s	Model 160 s
Temperature of silica gel at the inlet [°C]	41.0	40.3	42.2	41.6	43.2	42.8	44.6	44.4
Temperature of silica gel at the inlet [°C]	41.4	40.7	42.5	42.0	43.6	43.2	44.8	44.6
Adsorption								
	Exp. 30 s	Model 30 s	Exp. 60 s	Model 60 s	Exp. 90 s	Model 90 s		
Temperature of silica gel at the inlet [°C]	42.0	43.1	40.8	41.3	39.1	38.8		
Temperature of silica gel at the inlet [°C]	41.5	41.9	40.3	40.6	38.7	38.3		

The temperature of the silica gel is measured at the entrance and exit of the inclined bed until the temperature of the adsorbent stabilizes. In addition, the pressure in the tank that contains this moving bed is measured. Based on the experimental and simulation studies, it can be concluded that less compatibility between the obtained results of real and simulation studies was observed for the adsorption cycle (difference up to about 17%) than for the desorption cycle (difference up to about 13%). It should be noted here that the desorption time of the process even in stationary beds is longer than the adsorption time. Taking into account all the elements of a moving bed, it takes more time for the temperature to reach the value throughout the adsorbent, which also influences the desorption rate.

4. Discussion

The aim of the study was to compare the heating and cooling times of the sorbent in the bed at the same temperatures and pressures in the process of sorption and desorption as in the case of a mechanical bed and a stationary bed. The silica gel was used for this purpose, with the same parameters as in the case of the modification process and tests on a mechanical fluidal bed. This study will enable the verification of the thesis related to the possibility of using fluidal beds in the chiller, which has an increased impact on reducing the sorption and desorption time, and, consequently, increases the efficiency of the device.

Compare Stationary Bed during Adsorption Desorption Process with a Fluidal Mechanical Bed

In the adsorption chiller (Figure 8) installed at the at the Energy Centre of the AGH University of Science and Technology, operating in a three-bed system, one finned heat exchanger was installed in Tichelman scheme for each of the beds. The geometry of the exchanger consisted of two longitudinal manifolds connected by six tubes of smaller diameter, forming a meandering ‘finning’ to increase the heat transfer surface, and the

amount of sorbent in one bed is 3 kg. This part of the exchanger was connected to the fin plates by means of a casing. The geometry of the exchanger is shown in Figure 9.

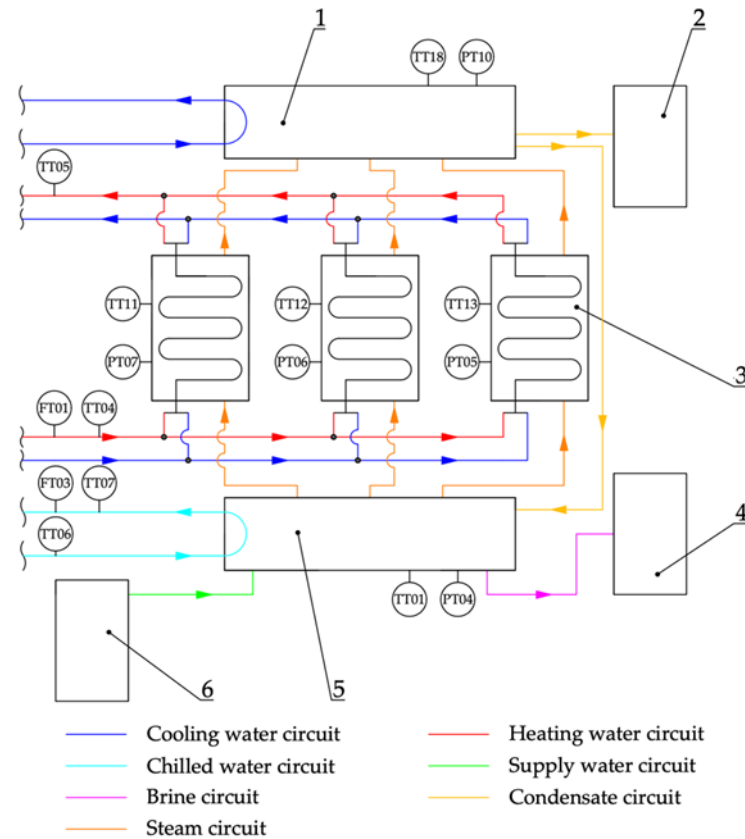


Figure 8. Scheme of the operation of adsorption chiller: 1—condenser; 2—distillate tank; 3—adsorbent bed; 4—brine tank; 5—evaporator; 6—deaerator; TT01—temperature in the evaporator; TT04—hot water inlet temperature [°]; TT05—hot water outlet temperature [°]; TT06—chilled water inlet temperature; TT07—chilled water outlet temperature; TT11—temperature in bed 1 [°]; TT12—temperature in bed 2 [°]; TT13—temperature in bed 3 [°]; TT18—temperature in the condenser [°]; PT04—pressure in the evaporator [kPa]; PT07—pressure in bed 1 [kPa]; PT06—pressure in bed 2 [kPa]; PT05—pressure in bed 3 [kPa]; PT10—pressure in the condenser [kPa]; FT01—hot water flow [L/min]; FT03—chilled water flow [L/min].

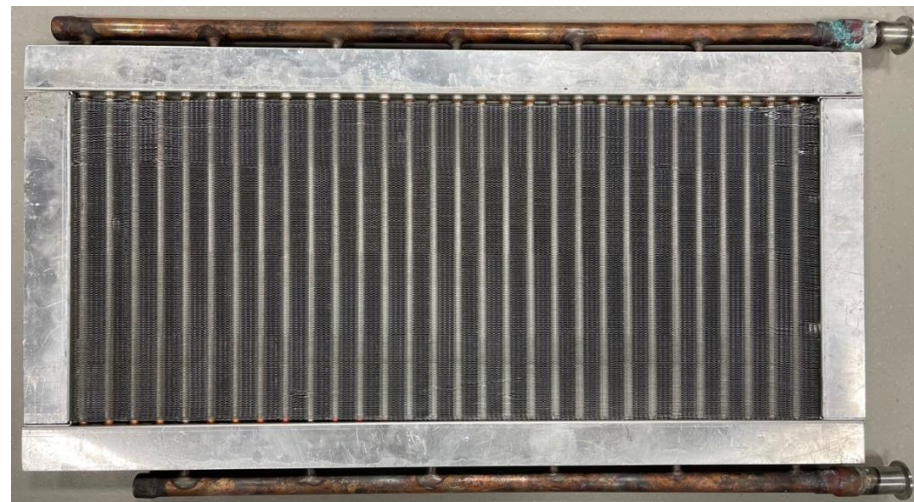


Figure 9. View of geometry of the heat exchanger in bed.

An analysis of the cooling time (adsorption process) of the sorbent in the bed was also carried out, consisting of a plate heat exchanger in the Tichelman system in an adsorption chiller installed at the Energy Centre of the AGH University of Science and Technology (CE AGH). As already mentioned, for the cooling of the bed, cooling water at a temperature of approx. 28 °C was used, which flows through a system of tubes in the heat exchanger of the bed heating the sorbent. Figure 10 shows the temperature drop of the sorbent in the heat exchanger as a function of time during the adsorption process when the cycle is switched.

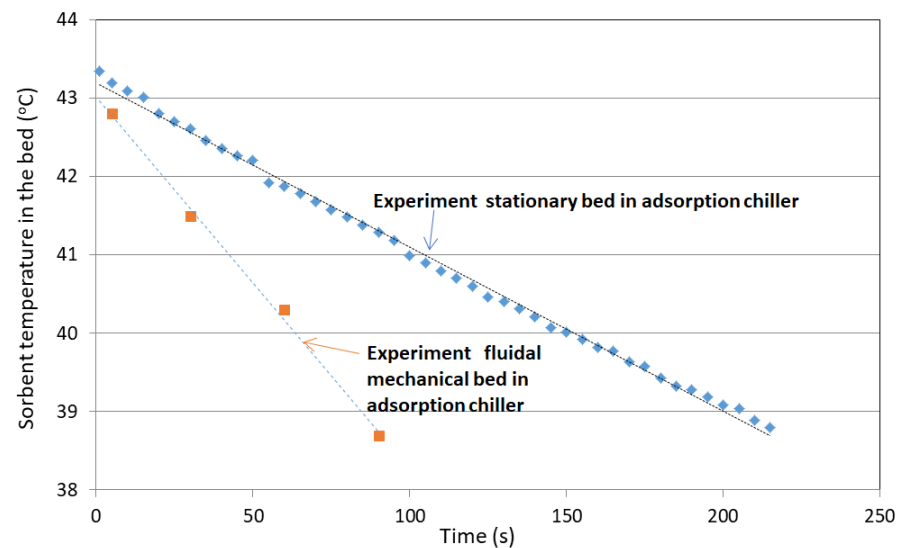


Figure 10. Comparison of change in the temperature of the sorbent during the adsorption process between stationary bed in an adsorption chiller at the CE AGH and fluidal mechanical bed of adsorption chiller as a function of time.

For the regeneration of the bed, hot water at a temperature of approx. 80 °C was used. Figure 11 shows the increase in temperature of the sorbent in the exchanger as a function of time during the desorption process when the cycle is switched over.

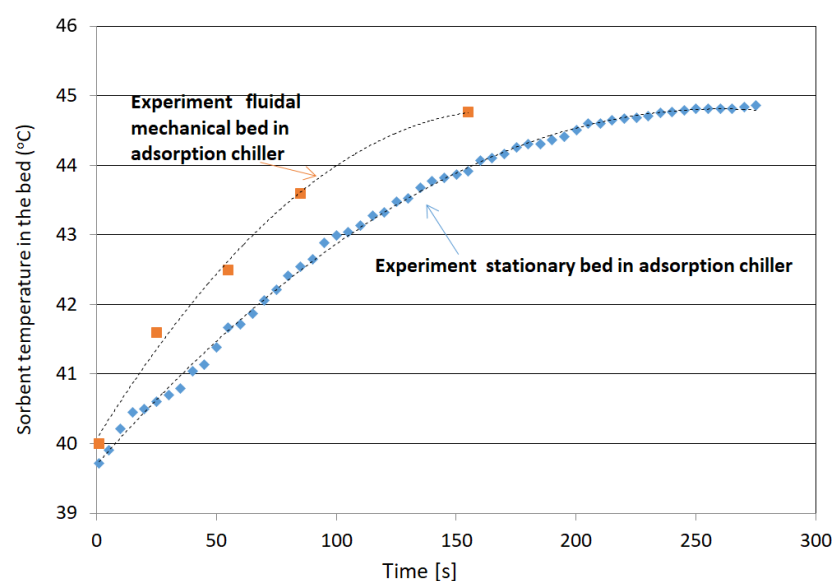


Figure 11. Comparison of the change in the temperature of the sorbent during the desorption process between stationary bed in an adsorption chiller at the CE AGH and fluidal mechanical bed of adsorption chiller as a function of time.

In a fixed-bed adsorption chiller, in the case of desorption with water at 80 °C, the increase in the temperature of the sorbent by $\Delta T = 4.78$ °C is reached only after approx. 200 s, while the whole desorption cycle for the experiment under consideration lasts 300 s. On the other hand, in the case of adsorption process using cooling water with a temperature of 28 °C, a decrease in the temperature of the sorbent by $\Delta T = 3.8$ °C is achieved only after approx. 190 s, while the whole adsorption cycle for the experiment conducted lasts 300 s. Such a long time of sorption/desorption is associated with the fixed packing of the sorbent in the heat exchanger, causing the heat transfer to be limited due to the low coefficient of thermal conductivity of the sorbent and of the material that the heat exchanger is made of. In the case of a fluidised bed, a temperature rise of $\Delta T = 4.78$ °C (desorption) is reached after approx. 12 s and a temperature drop of $\Delta T = 3.8$ °C (adsorption) is reached after approx. 12 s, which is associated with the intensive mixing of the sorbent material and the intensive washing of the surface of the heat exchanger. The shortening of the desorption/sorption time has a significant impact on increasing the capacity of the chiller and reducing its weight as the same amount of sorbent as is used in a fixed-bed chiller can generate several times higher cooling power in a fluidised bed cooler. The temperature rise in a fluidised bed is the result of a number of factors, such as contact time with the heat exchanger, contact time with the environment (when the medium circulates), velocity, frequency of collisions between the particles, etc.

The results of the model-based testing of the fluidised bed chiller confirm the literature data where the heat transfer in a fluidised bed can be up to 30 times better compared with that of a fixed bed. It is determined that the adsorption/desorption cycle in this type of the device is several times (more than 6.5 times) shorter than in a fixed bed, which is confirmed using data from model-based tests and literature data. It also contributes to improved contact between silica gel particles, which are in constant motion, and, consequently, to increased efficiency of adsorption and desorption. Fluidisation leads to an increase in the coefficient of heat transfer between the heat exchanger and the adsorbent, as well as an increase in the coefficient of thermal conductivity within the bed, the result of which is an improvement in the performance coefficients of the whole device. Inside the fluidised bed, single points with a higher temperature are rapidly dissipated, and the bed is characterised by a uniform temperature distribution. Rapid temperature equalization takes place throughout the bed. This makes it easier to control the temperature in the bed. This is a great advantage of fluidised beds as this cannot be achieved in fixed beds.

The fluidisation of silica gel particles can only take place under the right conditions. Of particular importance are the flow rate of the adsorbate and the size of the adsorbent particles affecting the weight and the number of voids inside the bed.

Based on the data modelled for the fixed bed instance and on literature data [25], it can be concluded that the adsorption and desorption capacity for a fluidised bed can be increased by approx. 23% and 20%, respectively, compared with a fixed bed packed with silica gel. On the basis of the literature review and the model-based testing, it can be concluded that in the case of the application of fluidised beds system in sorption systems, it is possible to increase the performance of adsorption refrigeration systems. The increase in the performance of adsorption chillers with fluidised beds is due to the following:

- An increase in adsorbed water by approx. 20% compared with fixed beds;
- The amount of desorbed water is approx. 16% greater than in the case of fixed beds.

The adsorption cycle for fluidal mechanical bed is up to 1.75 and the desorption process up to 1.2 times shorter than for stationary beds. This is due to the fact of increased possibility of adsorption of water vapour at the same amount as that of sorbent and the shortening of the adsorption–desorption cycle even. In addition, due to the fact that the heat exchange for a fluidised bed is 30 times higher than that for a fixed bed, it is possible to use heating water with a temperature below 60 °C for bed regeneration, the reason being the increased efficiency of heat exchange between the material and the heat exchanger through which the heating/cooling medium flows. The increased efficiency of the system will contribute to a reduction in the size of the unit and a reduction in the weight.

5. Conclusions

The technology of bed fluidisation is still being developed. Among other things, fluidisation contributes to the increase in the performance of adsorption chillers and makes it possible to reduce their size and weight. This will increase the attractiveness and competitiveness of this type of equipment in the refrigeration sector.

- The application of chillers with fluidised beds will open up the possibility to use the devices in all places where water with a temperature below 55–75 °C is available.
- The use of fluidised systems will reduce the weight (approx. 45%) and dimensions of the device (approx. 67%), which will result in a reduction in capital expenditure (approx. 30–40%) and the possibility of installing it in places where it was previously impossible to install the equipment due to its dimensions and weight.
- Fluidisation of the bed material in the chiller increases heat and mass transfer within the bed.
- The intensive motion of the sorbent particles in the fluidised bed within the heat exchanger has a significant effect on increasing the efficiency of the device.
- On the basis of model-based testing for the system fluidised bed, it can be stated that the heat transfer coefficients for this bed reach values above 0.4 W/(m²K).

The use of adsorption technologies enables the recovery of waste heat and, as a result, the production of cooling energy and/or distilled water.

- The advantage of sorption devices is the option of cascade configuration thanks to which the heating medium, after giving up the necessary heat in another sorption device, and after cooling, has the right temperature to supply another sorption device.
- The fluidised bed adsorption chiller is a functional device which enables the production of chilled water for technological and air-conditioning purposes as well as the desalination of saline water (seawater, brine, and post-process water), the operating principle of which is based on sorption processes.
- The chiller, due to its increased performance, enables a higher production of condensate in the process of desalination of saltwater compared with a fixed-bed chiller using the same sorbent mass.

Fluidised bed chillers represent a state-of-the-art solution that is superior to fixed-bed chillers, making it possible to use this type of technology on a larger scale.

Author Contributions: Conceptualization, K.S. and W.K.; methodology, W.K., K.S. and W.N.; validation, W.K., K.S. and A.M.-M.; formal analysis, E.R., K.S., W.N. and A.M.-M.; investigation, W.K., K.S., E.R. and A.M.-M.; resources, W.N. and L.M.; data curation, W.K., E.R., A.M.-M., L.M., T.B. and P.B.; writing—original draft preparation, W.K., K.S., E.R. and L.M.; writing—review and editing, K.S., E.R., A.M.-M., W.K., L.M., T.B. and P.B.; visualization, A.M.-M., E.R., T.B. and P.B.; supervision, W.N. and L.M.; project administration, L.M., W.N. and K.S.; funding acquisition, L.M., W.N. and K.S. All authors have read and agreed to the published version of the manuscript.

Funding: This research was funded by the Ministry of Science and Higher Education, Poland, Grant AGH No. 16.16.210.476, and partly supported by the program “Excellence initiative—research university” for the AGH University of Science and Technology.

Data Availability Statement: Not applicable.

Conflicts of Interest: The authors declare no conflict of interest.

References

1. IEA (International Energy Agency). *Key World Energy Statistics 2020*; International Energy Agency: Paris, France, 2020; Volume 33, p. 4649.
2. Stefański, S.; Nowak, W.; Sztékler, K.; Kalawa, W.; Siwek, T. Applicability of Adsorption Cooling/Desalination Systems Driven by Low-Temperature Waste Heat. *IOP Conf. Ser. Earth Environ. Sci.* **2019**, *214*, 012126. [[CrossRef](#)]
3. Sztékler, K.; Kalawa, W.; Nowak, W.; Mika, L.; Gradziel, S.; Krzywanski, J.; Radomska, E. Experimental Study of Three-Bed Adsorption Chiller with Desalination Function. *Energies* **2020**, *13*, 5827. [[CrossRef](#)]

4. Choudhury, B.; Saha, B.B.; Chatterjee, P.K.; Sarkar, J.P. An Overview of Developments in Adsorption Refrigeration Systems towards a Sustainable Way of Cooling. *Appl. Energy* **2013**, *104*, 554–567. [[CrossRef](#)]
5. Fernandes, M.S.; Brites, G.J.V.N.; Costa, J.J.; Gaspar, A.R.; Costa, V.A.F. Review and Future Trends of Solar Adsorption Refrigeration Systems. *Renew. Sustain. Energy Rev.* **2014**, *39*, 102–123. [[CrossRef](#)]
6. Grabowska, K.; Krzywanski, J.; Nowak, W.; Wesolowska, M. Construction of an Innovative Adsorbent Bed Configuration in the Adsorption Chiller-Selection Criteria for Effective Sorbent-Glue Pair. *Energy* **2018**, *151*, 317–323. [[CrossRef](#)]
7. Younes, M.M.; El-Sharkawy, I.I.; Kabeel, A.E.; Saha, B.B. A Review on Adsorbent-Adsorbate Pairs for Cooling Applications. *Appl. Therm. Eng.* **2017**, *114*, 394–414. [[CrossRef](#)]
8. Thu, K.; Saha, B.B.; Chua, K.J.; Ng, K.C. Performance Investigation of a Waste Heat-Driven 3-Bed 2-Evaporator Adsorption Cycle for Cooling and Desalination. *Int. J. Heat Mass Transf.* **2016**, *101*, 1111–1122. [[CrossRef](#)]
9. Sztékler, K.; Kalawa, W.; Mika, Ł.; Mlonka-Medrała, A.; Sowa, M.; Nowak, W. Effect of Additives on the Sorption Kinetics of a Silica Gel Bed in Adsorption Chiller. *Energies* **2021**, *14*, 1083. [[CrossRef](#)]
10. Stefański, S.; Mika, Ł.; Sztékler, K.; Kalawa, W.; Lis, Ł.; Nowak, W. Adsorption Bed Configurations for Adsorption Cooling Application. *E3S Web Conf.* **2019**, *108*, 01010. [[CrossRef](#)]
11. Sztékler, K.; Kalawa, W.; Mika, Ł.; Sowa, M. Effect of Metal Additives in the Bed on the Performance Parameters of an Adsorption Chiller with Desalination Function. *Energies* **2021**, *14*, 7226. [[CrossRef](#)]
12. Chua, H.T.; Ng, K.C.; Malek, A.; Kashiwagi, T.; Akisawa, A.; Saha, B.B. Multi-Bed Regenerative Adsorption Chiller-Improving the Utilization of Waste Heat and Reducing the Chilled Water Outlet Temperature Fluctuation. *Int. J. Refrig.* **2001**, *24*, 124–136. [[CrossRef](#)]
13. Krzywanski, J.; Grabowska, K.; Herman, F.; Pyrka, P.; Sosnowski, M.; Prauzner, T.; Nowak, W. Optimization of a Three-Bed Adsorption Chiller by Genetic Algorithms and Neural Networks. *Energy Convers. Manag.* **2017**, *153*, 313–322. [[CrossRef](#)]
14. Krzywanski, J.; Grabowska, K.; Sosnowski, M.; Zylka, A.; Kulakowska, A.; Czakiert, T.; Sztékler, K.; Wesolowska, M.; Nowak, W. Heat Transfer in Adsorption Chillers with Fluidized Beds of Silica Gel, Zeolite, and Carbon Nanotubes. *Heat Transf. Eng.* **2022**, *43*, 172–182. [[CrossRef](#)]
15. Thu, K.; Ng, K.C.; Saha, B.B.; Chakraborty, A.; Koyama, S. Operational Strategy of Adsorption Desalination Systems. *Int. J. Heat Mass Transf.* **2009**, *52*, 1811–1816. [[CrossRef](#)]
16. Wang, D.C.; Li, Y.H.; Li, D.; Xia, Y.Z.; Zhang, J.P. A Review on Adsorption Refrigeration Technology and Adsorption Deterioration in Physical Adsorption Systems. *Renew. Sustain. Energy Rev.* **2010**, *14*, 344–353. [[CrossRef](#)]
17. Ng, K.C.; Thu, K.; Kim, Y.; Chakraborty, A.; Amy, G. Adsorption Desalination: An Emerging Low-Cost Thermal Desalination Method. *Desalination* **2013**, *308*, 161–179. [[CrossRef](#)]
18. Wang, Q.; Gao, X.; Xu, J.Y.; Maiga, A.S.; Chen, G.M. Experimental Investigation on a Fluidized-Bed Adsorber/Desorber for the Adsorption Refrigeration System. *Int. J. Refrig.* **2012**, *35*, 694–700. [[CrossRef](#)]
19. Zhu, L.Q.; Tso, C.Y.; Chan, K.C.; Wu, C.L.; Chao, C.Y.H.; Chen, J.; He, W.; Luo, S.W. Experimental Investigation on Composite Adsorbent—Water Pair for a Solar-Powered Adsorption Cooling System. *Appl. Therm. Eng.* **2018**, *131*, 649–659. [[CrossRef](#)]
20. Engelprecht, M.; Gibelhaus, A.; Seiler, J.; Graf, S.; Nasruddin, N.; Bardow, A. Upgrading Waste Heat from 90 to 110 °C: The Potential of Adsorption Heat Transformation. *Energy Technol.* **2021**, *9*, 2000643. [[CrossRef](#)]
21. Horibe, A.; Haruki, N.; Hiraishi, D. Sorption-Desorption Operations on Two Connected Fluidized Bed Using Organic Sorbent Powder. *Int. J. Heat Mass Transf.* **2013**, *65*, 817–825. [[CrossRef](#)]
22. Eflita, Y.; Ismoyo, H.; Muhamad Adrian, D.; Yusuf, L.H. Static and Dynamic Analysis of Vibro Fluidized Bed Dryer Using Finite Element Method. *E3S Web Conf.* **2018**, *73*, 3–6. [[CrossRef](#)]
23. Rogala, Z.; Kolański, P.; Gnutek, Z. Effect of Operating Conditions on Performance of Silica Gel-Water Air-Fluidised Desiccant Cooler. *E3S Web Conf.* **2017**, *22*, 00146. [[CrossRef](#)]
24. Nikam, S.; Mandal, D. A Study on Fluidization of Activated Carbon Particles in Gas-Solid Fluidized Bed. *Indian. Chem. Eng.* **2021**, *63*, 478–490. [[CrossRef](#)]
25. Chen, C.H.; Ma, S.S.; Wu, P.H.; Chiang, Y.C.; Chen, S.L. Adsorption and Desorption of Silica Gel Circulating Fluidized Beds for Air Conditioning Systems. *Appl. Energy* **2015**, *155*, 708–718. [[CrossRef](#)]
26. Hamed, A.M.; Abd El Rahman, W.R.; El-Eman, S.H. Experimental Study of the Transient Adsorption/Desorption Characteristics of Silica Gel Particles in Fluidized Bed. *Energy* **2010**, *35*, 2468–2483. [[CrossRef](#)]
27. Chen, C.H.; Schmid, G.; Chan, C.T.; Chiang, Y.C.; Chen, S.L. Application of Silica Gel Fluidised Bed for Air-Conditioning Systems. *Appl. Therm. Eng.* **2015**, *89*, 229–238. [[CrossRef](#)]
28. Hamed, A.M. Experimental Investigation on the Adsorption/Desorption Processes Using Solid Desiccant in an Inclined-Fluidized Bed. *Renew. Energy* **2005**, *30*, 1913–1921. [[CrossRef](#)]
29. Llop, M.F.; Madrid, F.; Arnaldos, J.; Casal, J. Fluidization at Vacuum Conditions. A Generalized Equation for the Prediction of Minimum Fluidization Velocity. *Chem. Eng. Sci.* **1996**, *51*, 5149–5157. [[CrossRef](#)]
30. Crowe, C.T.; Schwarzkopf, J.D.; Sommerfeld, M.; Tsuj, Y. *Multi-Phase Flows with Droplets and Particles*; CRC Press: Boca Raton, FL, USA, 1998; ISBN 9781439840511.
31. ANSYS, Inc. *ANSYS Fluent Theory Guide*; ANSYS, Inc.: Canonsburg, PA, USA, 2021.

32. Adamczyk, W.P.; Klimanek, A.; Białecki, R.A.; Węcel, G.; Kozołub, P.; Czakiert, T. Comparison of the Standard Euler–Euler and Hybrid Euler–Lagrange Approaches for Modeling Particle Transport in a Pilot-Scale Circulating Fluidized Bed. *Particuology* **2014**, *15*, 129–137. [[CrossRef](#)]
33. Magnussen, B.F.; Hjertager, B.H. On Mathematical Modeling of Turbulent Combustion with Special Emphasis on Soot Formation and Combustion. In *Symposium (International) on Combustion*; Elsevier: Amsterdam, The Netherlands, 1977; Volume 16, pp. 719–729. [[CrossRef](#)]
34. Menter, F.R. Two-Equation Eddy-Viscosity Turbulence Models for Engineering Applications. *AIAA J.* **1994**, *32*, 1598–1605. [[CrossRef](#)]
35. Sztekler, K.; Kalawa, W.; Nowak, W.; Mika, L.; Krzywanski, J.; Grabowska, K.; Sosnowski, M.; Alharbi, A. Performance Evaluation of a Single-Stage Two-Bed Adsorption Chiller With Desalination Function. *J. Energy Resour. Technol.* **2021**, *143*, 082101. [[CrossRef](#)]
36. Sztekler, K.; Siwek, T.; Kalawa, W.; Lis, L.; Mika, L.; Radomska, E.; Nowak, W. CFD Analysis of Elements of an Adsorption Chiller with Desalination Function. *Energies* **2021**, *14*, 215. [[CrossRef](#)]

Disclaimer/Publisher’s Note: The statements, opinions and data contained in all publications are solely those of the individual author(s) and contributor(s) and not of MDPI and/or the editor(s). MDPI and/or the editor(s) disclaim responsibility for any injury to people or property resulting from any ideas, methods, instructions or products referred to in the content.